Journal of Materials Chemistry C

PAPER

View Article Online
View Journal | View Issue



Cite this: J. Mater. Chem. C, 2014, 2, 10129

# New sulfone-based electron-transport materials with high triplet energy for highly efficient blue phosphorescent organic light-emitting diodes†

Soon Ok Jeon, Taeshik Earmme and Samson A. Jenekhe*

A series of new electron transport materials, which combines a diphenylsulfone core with different electron withdrawing end groups, has been synthesized, characterized, and found to exhibit high triplet energy ($E_T$ > 2.8 eV) for use in phosphorescent organic light emitting diodes (PhOLEDs). The new materials, including 3,3′-(4,4′-sulfonylbis(4,1-phenylene))dipyridine (**SPDP**), 5,5′-(4,4′-sulfonylbis(4,1-phenylene)) bis(3-phenylpyridine) (**SPPP**), and 3,3′-(4,4′-sulfonylbis(4,1-phenylene))diquinoline (**SPDQ**) had wide band gaps (3.6–3.8 eV) and LUMO levels of −2.4 to −2.7 eV. The triplet energy measured from phosphorescence spectra at 77 K varied from 2.53 eV for **SPDQ** and 2.81 eV for **SPPP** to 2.90 eV for **SPDP**, which are in good agreement with density functional theory calculated values. High performance blue PhOLEDs using the sulfone-based materials are exemplified by devices containing a poly(*N*-vinylcarbazole) host and **SPDP** electron transport layer, which had a high quantum efficiency (19.6%) and a high current efficiency (33.6 cd $A^{-1}$) even at very high luminances (4500 cd $m^{-2}$). These results demonstrate that sulfone-based molecules are promising electron transport materials for application in developing highly efficient phosphorescent OLEDs.

Received 8th July 2014
Accepted 14th October 2014

DOI: 10.1039/c4tc01474j

www.rsc.org/MaterialsC



## Introduction

Organic light-emitting diodes (OLEDs) are finding applications in full-color flat panel displays, flexible displays, and solid-state lighting.[1] Recent research on OLEDs has largely focused on developing new materials and device strategies for achieving highly efficient phosphorescent organic light-emitting diodes (PhOLEDs) because nearly 100% internal quantum efficiency can be realized.[2] One promising strategy towards highly efficient PhOLEDs is through the utilization of high triplet energy materials to confine triplet excitons inside the emission layer (EML) in multilayered device structures.[3–5]

High-performance PhOLEDs[4–12] and OLEDs[13,14] have been achieved by using various classes of electron-transport materials (ETMs)[7] such as pyridine,[8a] phenylpyrimidine,[8b] triazine,[9] quinoline[10] and phosphine oxide (PO) derivatives.[11,12] Phosphine-oxide-based ETMs have gained much attention due to their good exciton blocking ability enabled by their high triplet energy.[6] The PO group is known to lower the LUMO level predominantly by inductive electron-withdrawing effect, which facilitates electron-injection while retaining high triplet energy. The sulfonyl group ($SO_2$) is another attractive group with good electron withdrawing properties comparable to the phosphine oxide (PO) group. Sulfone-based materials can be expected to have efficient electron-injection and transport due to the strong electron withdrawing character of the disulfoxide group and the high triplet energy and wide band gap of the materials. They are also known to have good electrochemical and thermal stability.[13,14]

High triplet energy materials containing the sulfone group were reported for applications in PhOLEDs. Hsu *et al.* reported bis(phenylsulfonyl)fluorine-based molecule as the host material for red PhOLEDs.[15] Recently, Marder and Kippelen *et al.* synthesized and evaluated a bis(phenylsulfonyl)biphenyl molecule,[16] and Kido *et al.* reported a sulfone derivative as a high triplet energy (calcd. $E_T = 3.11$ eV) host material for bis(3,5-difluoro-2-(2-pyridyl)phenyl-(2-carboxypyridyl)iridium) (FIrpic) triplet emitter in blue PhOLEDs.[17] More recently, Adachi *et al.* demonstrated diphenylsulfone-core structured molecules for efficient thermally activated delayed fluorescence (TADF) blue emitting materials.[18] However, all previous reports on sulfone-based materials to date have focused on their use as host or emitting materials for PhOLEDs,[15–18] which involves vacuum co-deposition of the materials.

In this paper, we report the synthesis, experimental and theoretical electronic structure, photophysics, and thermal and electron-transport properties of a series of new sulfone-based high triplet energy materials and demonstrate their use as efficient electron transport materials in high performance blue PhOLEDs. The new electron transport materials (ETMs) include 3,3′-(4,4′-sulfonylbis(4,1-phenylene))dipyridine (**SPDP**),

*Department of Chemical Engineering and Department of Chemistry, University of Washington, Seattle, WA 98195-1750, USA. E-mail: jenekhe@u.washington.edu*

† Electronic supplementary information (ESI) available: TGA thermograms and cyclic voltammograms of sulfone-based ETMs. See DOI: 10.1039/c4tc01474j

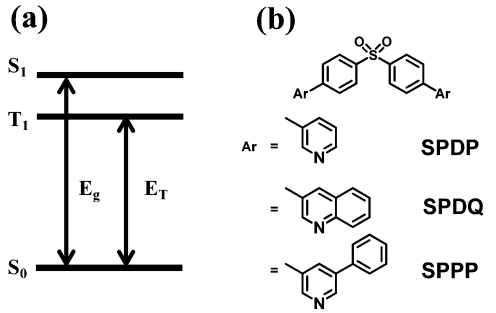


Chart 1 Diagram of (a) singlet energy ($S_1$) and triplet energy ($T_1$) and (b) diphenylsulfone core structure with different substituents.



5,5′-(4,4′-sulfonylbis(4,1-phenylene))bis(3-phenylpyridine) (**SPPP**), and 3,3′-(4,4′-sulfonylbis(4,1-phenylene))diquinoline (**SPDQ**). The new sulfone-based ETMs, whose molecular structures are shown in Chart 1, have a diphenylsulfone core with different electron withdrawing substituents (pyridine, phenylpyridine, and quinoline) aimed at controlling the triplet energy ($E_T$), band gap ($E_g$) and electron transport properties. The triplet energy ($E_T$) of the new electron transport materials was measured from the low temperature (77 K) phosphorescence spectra and compared to density functional theory (DFT) based predicted values. The electron mobility of the ETMs was measured in space-charge limited current (SCLC) experiments on evaporated thin films. Finally, a series of blue PhOLEDs was fabricated and evaluated toward investigation of the electron transport and exciton blocking properties of the new sulfone-based ETMs. The results demonstrate that the new sulfone-based molecules are promising electron transport materials with high triplet energy for high-performance PhOLEDs.

# Experimental

## Materials

Bis(4-chlorophenyl) sulfone, 3-pyridinylboronic acid, quinoline-3-boronic acid, phenylboronic acid, tetrakis(triphenylphosphine) palladium(0), potassium carbonate, 3,5-dibromopyridine, *n*-butyllithium, 1,4-dioxane, trimethyltin chloride, copper iodide, anhydrous toluene and tetrahydrofuran (Aldrich) were used without further purification.

### Synthesis 3-bromo-5-phenylpyridine (1)

A mixture of 3,5-dibromopyridine (5.0 g, 21.1 mmol), phenylboronic acid (3.08 g, 25.3 mmol) and tetrakis(triphenylphosphine)palladium(0) (5 mol%) in 80 mL of 1,4-dioxane was refluxed under argon for 12 h. To the reaction mixture was added slowly a solution of potassium carbonate (2 M, 80 mL). After cooling to room temperature, the reaction mixture was extracted with dichloromethane and water. The organic layer was evaporated with a rotary evaporator. The product was purified by column chromatography using ethyl acetate and hexane mixture (10 : 90) and a white solid product was obtained (3.5 g, 72% yield). $^1$H NMR (300 MHz, $CDCl_3$, ppm): $\delta$ 8.74–8.64 (d, 2H), 7.99 (s, 1H), 7.54–7.38 (m, 5H).

### 4,4′-Sulfonylbis(4,1-phenylene)bis(trimethylstannane) (2)

To a solution of bis(4-chlorophenyl) sulfone (3.0 g, 10.4 mmol) in 50 mL anhydrous tetrahydrofuran, 2.5 M solution of *n*-BuLi (9.19 mL, 22.9 mmol) was added dropwise at −78 °C. The solution was stirred at −78 °C for 2 h and 1.0 M solution of trimethyltin chloride (22.9 mL, 22.9 mmol) in tetrahydrofuran was added. The solution was warmed to room temperature and 50 mL of water and 50 mL of ethyl ether were added. The organic layer was washed twice with 50 mL of water and dried over anhydrous $MgSO_4$. The organic layer was evaporated and dried over vacuum to afford white solid (5.5 g, 97% yield). $^1$H NMR ($CDCl_3$, 300 MHz, ppm): $\delta$ 7.72–7.66 (m, 4H), 7.34–7.28 (m, 4H), 0.42 (s, 18H).

### 3,3′-(4,4′-Sulfonylbis(4,1-phenylene))dipyridine (SPDP)

A mixture of bis(4-chlorophenyl) sulfone (2.0 g, 6.96 mmol), 3-pyridinylboronic acid (1.02 g, 8.35 mmol) and tetrakis(triphenylphosphine)palladium(0) (5 mol%) in 20 mL of anhydrous tetrahydrofuran was refluxed under argon for 12 h. To the reaction mixture was slowly added a solution of potassium carbonate (2 M, 20 mL). After cooling to ambient temperature, the reaction mixture was extracted with dichloromethane and water. The organic layer was evaporated with a rotary evaporator. The product was purified by column chromatography using ethyl acetate and *n*-hexane mixture (10 : 90) and a white solid product was obtained (1.65 g, 63% yield); $T_m$ 239 °C. $^1$H NMR (300 MHz, $CDCl_3$, ppm): $\delta$ 8.85 (s, 2H), 8.67 (s, 2H), 8.12–8.09 (d, 4H), 7.90–7.87 (d, 2H), 7.76–7.74 (d, 4H), 7.45–7.40 (m, 2H). $^{13}$C NMR (500 MHz, $CDCl_3$, ppm): $\delta$ 149.7, 148.3, 142.9, 141.0, 134.6, 128.5, 128.1, 123.7. MALDI-TOF/MS: 373 [$(M + H)^+$]. Anal. calcd. for $C_{22}H_{16}N_2O_2S$: C, 70.95; H, 4.33; N, 7.52; S, 8.61. Found: C, 70.99; H, 4.19; N, 7.50; S, 8.45.

### 5,5′-(4,4′-Sulfonylbis(4,1-phenylene))bis(3-phenylpyridine) (SPPP)

3-Bromo-5-phenylpyridine (**1**) (3.0 g, 12.8 mmol) and 4,4′-sulfonylbis(4,1-phenylene)bis(trimethylstannane) (**2**) (4.18 g, 7.68 mmol) and catalyst tetrakis(triphenylphosphine)palladium (0) (5 mol%) and copper iodide (1 mol%) in anhydrous toluene (30 mL) were heated at 120 °C for 24 h. The solution was warmed to room temperature and extracted with 50 mL of water and 50 mL of dichloromethane. The organic layer was dried over anhydrous $MgSO_4$. The product was purified by column chromatography using ethyl acetate and *n*-hexane mixture (10 : 40) and a white solid product was obtained. Yield 45%; $T_m$ 180 °C. $^1$H NMR ($CDCl_3$, 300 MHz, ppm): $\delta$ 8.93–8.90 (d, 4H), 8.12 (s, 2H), 7.69–7.47 (m, 18H). $^{13}$C NMR (500 MHz, $CDCl_3$, ppm): $\delta$ 148.0, 146.9, 137.3, 137.0, 133.4, 133.0, 129.3, 128.5, 127.3. MALDI-TOF/MS: 525 [$(M + H)^+$]. Anal. calcd. for $C_{34}H_{24}N_2O_2S$: C, 77.84; H, 4.61; N, 5.34; S, 6.11. Found: C, 77.90; H, 4.58; N, 5.31; S, 5.98.

### 3,3′-(4,4′-Sulfonylbis(4,1-phenylene))diquinoline (SPDQ)

A mixture of bis(4-chlorophenyl)sulfone (1.77 g, 6.10 mmol), quinoline-3-boronic acid (2.56 g, 14.7 mmol) and tetrakis(triphenylphosphine)palladium(0) (5 mol%) in 20 mL of

 

anhydrous tetrahydrofuran was refluxed under argon for 12 h. To the reaction mixture was slowly added a solution of potassium carbonate (2 M, 20 mL). After cooling to ambient temperature, the reaction mixture was extracted with dichloromethane and water. The organic layer was evaporated with a rotary evaporator. The product was purified by column chromatography using ethyl acetate and *n*-hexane mixture (10 : 90) and a white solid product was obtained (0.90 g, 32% yield); $T_m$ 229 °C. $^1$H NMR (300 MHz, $CDCl_3$, ppm): $\delta$ 9.17 (s, 2H), 8.35 (s, 2H), 8.20–8.10 (m, 4H), 7.98–7.78 (m, 8H), 7.67–7.62 (m, 2H), 7.55–7.53 (m, 2H). $^{13}$C NMR (500 MHz, $CDCl_3$, ppm): $\delta$ 149.2, 147.9, 143.1, 143.0, 140.9, 140.6, 140.1, 140.0, 134.1, 131.8, 130.3, 129.7, 129.3, 129.2, 128.6, 128.5, 128.3, 128.2, 127.7, 127.5. MALDI-TOF/MS: 473 [$(M + H)^+$]. Anal. calcd. for $C_{30}H_{20}N_2O_2S$: C, 76.25; H, 4.27; N, 5.93; S, 6.79. Found: C, 76.14; H, 4.21; N, 4.89; S, 7.34.

### General analysis

$^1$H NMR spectra were recorded on a Bruker AV300 at 300 MHz, whereas $^{13}$C NMR spectra were recorder on a Bruker AV500 at 500 MHz using $CDCl_3$ as the solvent. The MALDI-TOF mass spectra were recorded using a Bruker Autoflex II spectrometer. The ultraviolet-visible (UV-vis) absorption spectra were obtained by means of a Perkin-Elmer model Lambda 900 UV/vis/near-IR spectrophotometer and the photoluminescence (PL) spectra were recorded on a Photon Technology International (PTI) Inc. Model QM 2001-4 spectrofluorimeter. The UV-vis absorption and solution PL emission spectra of electron transport materials (ETMs) were obtained from dilute toluene solution, while the solid PL spectra were obtained from thin films prepared by vacuum evaporation. Triplet energy values of the ETMs were obtained from the photoluminescence spectra at 77 K using liquid nitrogen. The differential scanning calorimeter (DSC) measurements were performed on a TA Instruments Q100 under nitrogen at a heating rate of 10 °C min$^{-1}$ to measure the melting point ($T_m$) and glass transition temperature ($T_g$). Thermogravimetric analysis (TGA) was done on a TA Instruments Q50 under flowing nitrogen at a heating rate of 20 °C min$^{-1}$. The energy levels were measured by using cyclic voltammetry (CV). Each ETM was dissolved in anhydrous acetonitrile with 0.1 M tetrabutylammonium hexafluorophosphate as the electrolyte to measure the reduction CV from which the LUMO energy level was estimated. We used a platinum wire electrode both working and counter electrode and a saturated Ag/AgCl reference electrode. Ferrocene was used as the standard reference. All solutions were purged with nitrogen for 10 minutes before each experiment.

### Device fabrication and characterization

The phosphorescent emission layer (EML) consisted of a blend of poly(*N*-vinylcarbazole) (PVK) and 1,3-bis(2-(4-tert-butylphenyl)-1,3,4-oxadiazo-5-yl)benzene (OXD-7) (PVK : OXD-7 = 60 : 40, wt% : wt%) as a host and 10.0 wt% FIrpic as the blue dopant. A solution of Clevios P VP Al 4083 PEDOT:PSS (poly(ethylenedioxythiophene)-polystyrenesulfonate) as received, was filtered before spin-coating to make a 30 nm hole injection layer onto a precleaned ITO glass. Then the film was annealed at 150 °C under vacuum to remove residual water. The 70 nm polymer EML was obtained by spin coating of the PVK : OXD-7 : FIrpic blend in chlorobenzene onto the PEDOT:PSS layer and vacuum dried at 100 °C overnight. Sulfone-based ETM was vacuum-deposited onto the EML followed by deposition of 1 nm LiF and 100 nm Al cathode without breaking the vacuum. The device structure with different thickness of **SPDP** ETL:ITO/PEDOT:PSS/blue EML/**SPDP**/Al with 5, 15, and 30 nm thick **SPDP**. A set of blue PhOLEDs were also fabricated; device I: ITO/PEDOT:PSS/blue EML/LiF/Al; device II: ITO/PEDOT:PSS/blue EML/**SPDP** (15 nm) LiF/Al; device III: ITO/PEDOT:PSS/blue EML/**SPPP** (15 nm)/LiF/Al; and device IV: ITO/PEDOT:PSS/blue EML/**SPDQ** (15 nm)/LiF/Al.

Film thickness was measured by using an Alpha-Step 500 profilometer (KLA-Tencor, San Jose, CA). Electroluminescence (EL) spectra were obtained by using the same spectrofluorimeter described above. Device performance of the PhOLEDs was measured by using a HP4155A semiconductor parameter analyzer (Yokogawa Hewlett-Packard, Tokyo). The luminance was simultaneously measured by using a model 370 optometer (UDT Instruments, Baltimore, MD) equipped with a calibrated luminance sensor head (Model 211) and a 5× objective lens. The device external quantum efficiency (EQE) was calculated from the luminance, current density and EL spectrum assuming a Lambertian distribution using procedures reported previously.[19] All the device fabrication and device characterization steps were carried out under ambient laboratory conditions.

Devices for space-charge-limited current (SCLC) measurement were fabricated with single carrier device structure: ITO/sulfone-based ETM (100 nm)/Al. The 100 nm sulfone-based ETM was deposited onto the plasma cleaned ITO substrate followed by vacuum-deposition of Al electrode. Current density-voltage (*J*–*V*) characteristics of SCLC devices were measured using the same semiconductor parameter analyzer as for the characterization of PhOLEDs. The SCLC measurements were performed under dark and ambient conditions.

## Results and discussion

### Synthesis and characterization

The synthetic route to the new sulfone-based electron transport materials is shown in Scheme 1. The compounds, 3,3′-(4,4′-sulfonylbis(4,1-phenylene))dipyridine (**SPDP**) and 3,3′-(4,4′-

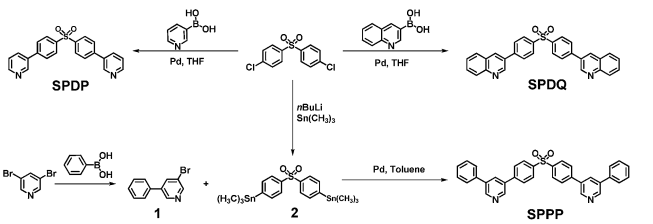


Scheme 1 Synthetic route of sulfone-based ETMs: **SPDP**, **SPDQ**, and **SPPP**.

sulfonylbis(4,1-phenylene))diquinoline (**SPDQ**), were synthesized by Suzuki coupling reaction of bis(4-chlorophenyl) sulfone with 3-pyridylboronic acid and quinoline-3-boronic acid, respectively using tetrakis(triphenylphosphine)palladium(0) in anhydrous tetrahydrofuran. The reaction of 3,5-dibromopyridine with phenylboronic acid in the presence of palladium catalyst in 1,4-dioxane gave 3-bromo-5-phenylpyridine (**1**) in 72% yield. 4,4′-Sulfonylbis(4,1-phenylene)bis(trimethylstannane) (**2**) was prepared by stannylation of bis(4-chlorophenyl) sulfone with 97% yield. The compound 5,5′-(4,4′-sulfonylbis(4,1-phenylene))bis(3-phenylpyridine) (**SPPP**) was synthesized by Stille coupling reaction between **1** and **2** with tetrakis(triphenylphosphine)palladium(0) and copper iodide in anhydrous toluene. The three final products (**SPDP**, **SPPP**, **SPDQ**) were purified by column chromatography and molecular structures were confirmed by $^{1}$H NMR, $^{13}$C NMR and elemental analysis.

Thermal properties of the sulfone-based ETMs were characterized by thermogravimetric analysis (TGA) and differential scanning calorimetry (DSC). TGA and DSC curves of the new sulfone-based ETMs are shown in Fig. S1 (ESI†) and 1, respectively. Numerical values extracted from the TGA and DSC scans are given in Table 1. Three distinct transitions were seen in the second-heating/cooling DSC scans of **SPDP**, **SPPP** and **SPDQ**. These materials showed a high melting point ($T_m$) of 239, 180 and 229 °C, respectively, whereas they did not exhibit a glass transition temperature ($T_g$) up to the $T_m$. The sulfone-based materials crystallize upon cooling from the melt. The **SPDP**, **SPPP** and **SPDQ** showed onset crystallization temperature ($T_c$) at 223, 146 and 197 °C, respectively. The onset decomposition temperature ($T_d$) of the new sulfone-based materials determined from TGA thermograms showed high values in the range of 386 to 453 °C, which demonstrate their thermal robustness.

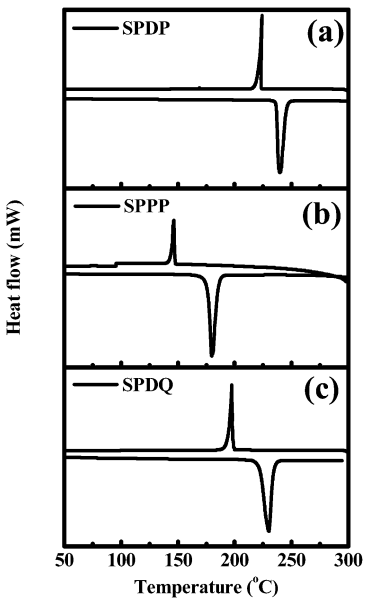


Fig. 1 DSC thermograms of sulfone-based ETMs: (a) SPDP; (b) SPPP; and (c) SPDQ.

The new ETMs are stable to temperatures above 350 °C. The fact that apparent complete thermal decomposition with zero% weight remaining is observed in the TGA curves suggests that the materials can be readily evaporated to form thin films.

## Photophysical properties

Optical absorption and photoluminescence (PL) spectra of the **SPDP**, **SPPP** and **SPDQ** molecules in dilute toluene solution ($5 \times 10^{-5}$ M) and thin films are shown in Fig. 2. The solid state absorption and PL emission spectra of **SPDP**, **SPPP** and **SPDQ** were obtained from thermally evaporated thin films. The key numerical values of the photophysical properties of the sulfone-based ETMs, including absorption maximum ($\lambda_{max}^{abs}$), molar absorption coefficient (log $\varepsilon$), PL emission maximum ($\lambda_{max}^{em}$) and optical band gap ($E_g$) are summarized in Table 1. A strong solution absorption peak was observed between 281 nm and 298 nm which is assigned to the absorption of the diphenylsulfone unit in the molecules. Similar absorption spectra were observed in the three ETMs due to the common diphenylsulfone core in the molecules. In the case of **SPDP**, it showed an absorption maximum ($\lambda_{max}^{abs}$) at 285 nm (log $\varepsilon$ = 4.33). The thin film absorption spectrum has a similar line shape except that $\lambda_{max}^{abs}$ is at 296 nm. **SPPP** has an absorption with a maximum centered at 281 nm (log $\varepsilon$ = 4.36) in solution but red shifts to 289 nm in thin film. The absorption spectrum of the quinoline functionalized ETM, **SPDQ**, has a $\lambda_{max}^{abs}$ at 298 nm (log $\varepsilon$ = 3.47) in solution. However, the absorption spectrum of **SPDQ** thin films showed two absorption peaks at 279 nm and 306 nm; the latter $\lambda_{max}^{abs}$ value originates from quinoline ring.[10] The red-shift of the π–π* band between solution and thin film was 11 nm for **SPDP**, indicating an increase in electron delocalization in the bulk solid state. In addition, the π–π* band in **SPPP** and **SPDQ** in both dilute solution and thin film is red-shifted by 8 nm compared to that of **SPDP**. This means that the extent of electron delocalization is greater with phenylpyridine and quinoline than with the pyridine. The PL emission maximum ($\lambda_{max}^{em}$) of **SPDP**, **SPPP** and **SPDQ** was observed at 291, 294 and 375 nm, respectively. The emission maximum is red-shifted with increasing π-conjugation. Optical band gaps of **SPDP**, **SPPP** and **SPDQ** were estimated from the absorption edge of the UV-vis spectra, revealing $E_g$ of 3.6, 3.79 and 3.64 eV, respectively.

The triplet energy ($E_T$) of the new ETMs was estimated from the shortest wavelength emission peak of the phosphorescence spectrum obtained at low temperature (77 K) in dilute 2-methyl tetrahydrofuran solution. The phosphorescent spectra of the sulfone-based ETMs are shown in Fig. 3. The measured triplet energies of the three ETMs are given in Table 1. In the case of **SPDP** and **SPPP**, their $E_T$ values of 2.90 eV and 2.81 eV, respectively, are high enough to confine the triplet excitons of blue emitting FIrpic which has a triplet energy of 2.7 eV.[10] These triplet energy values are much higher than those of commercial ETMs, such as 2,9-dimethyl-4,7-diphenyl-1,10-phenanthroline (BCP) ($E_T$ = 2.5 eV).[20] The $E_T$ value of **SPDQ** (2.53 eV), which is comparable to that of BCP, is too low to confine the triplet excitons of blue emitters but could be more useful for green and red triplet emitters.

 

Table 1 Thermal and photophysical properties of sulfone-based ETMs

| | | | $\lambda_{max}^{abs}$ (nm) | | | $\lambda_{max}^{em}$ (nm) | | | | |
|---|---|---|---|---|---|---|---|---|---|---|
| ETM | $T_m$ (°C) | $T_d$ (°C) | Solution | log $\varepsilon$ ($M^{-1}$ $cm^{-1}$) | Film | Solution | Film | HOMO/LUMO (eV) | $E_g$ (eV) | $E_T$ (eV) |
| **SPDP** | 239 | 386 | 285 | 4.33 | 296 | 291 | 399 | −6.17/−2.57 | 3.60 | 2.90 |
| **SPPP** | 180 | 342 | 281 | 4.36 | 289 | 294 | 393 | −6.16/−2.37 | 3.79 | 2.81 |
| **SPDQ** | 229 | 453 | 298 | 3.47 | 279, 306 | 375 | 409 | −6.32/−2.7 | 3.64 | 2.53 |

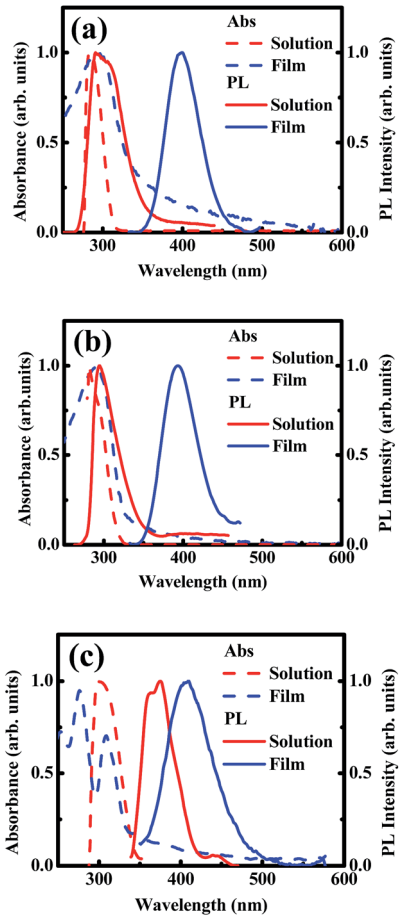


Fig. 2 Normalized absorption and PL emission spectra of sulfone-based ETMs in dilute toluene solution ($5 \times 10^{-5}$ M) and thin solid films: (a) SPDP; (b) SPPP; and (c) SPDQ.

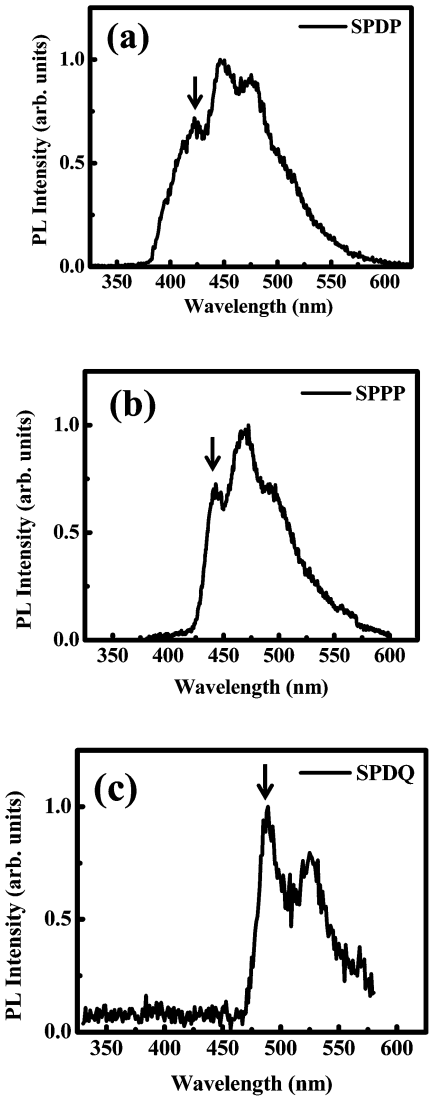


Fig. 3 Normalized phosphorescence spectra of sulfone-based ETMs at 77 K: (a) SPDP; (b) SPPP; and (c) SPDQ.

### Cyclic voltammetry and electronic structure

Electronic structure (LUMO/HOMO energy levels) of the sulfone-based ETMs was studied by cyclic voltammetry (CV). The cyclic voltammograms of the ETMs in solution are shown in Fig. S2 (ESI†). **SPDP** show two reversible reduction waves whereas the reduction CVs of **SPPP** and **SPDQ** were not reversible. The onset reduction potentials ($E_{red}^{onset}$) of the sulfone-based ETMs **SPDP**, **SPPP** and **SPDQ** are −1.83, −2.03 and −1.7 V (*vs.* SCE), respectively. The LUMO energy levels of the ETMs were obtained according to the equation $E_{LUMO} = eE_{red}^{onset} + 4.4$ eV,[21] using ferrocene as the internal standard. The LUMO levels of **SPDP**, **SPPP** and **SPDQ** were found to be −2.57, −2.37 and −2.7 eV, respectively. Oxidation CV was not observed for any of the sulfone-based materials. The HOMO levels of **SPDP**, **SPPP** and **SPDQ** were found to be −6.17, −6.16 and −6.32 eV, respectively, as estimated from the difference between the LUMO level and the optical band gap ($E_g$). The HOMO levels of **SPDP** and **SPPP** are similar to those of other ETMs with deep HOMO level such as BCP (−6.1 eV) or 4,7-diphenyl-1,10-phenanthroline (BPhen) (−6.2 eV).[4a] Similar with BCP and Bphen, we believe that the

low-lying HOMO energy levels of the new materials suggest good exciton and hole blocking properties. The LUMO/HOMO energy levels of the sulfone-based ETMs are shown together in Fig. 4.

### Molecular simulation of the sulfone-based ETMs

The results of molecular simulations of the new sulfone-based ETMs are shown in Fig. 5. The *ab initio* calculations were performed using a suite of Gaussian programs.[22] Molecular structures of the **SPDP**, **SPPP** and **SPDQ** were optimized by density functional theory (DFT) using Becke's three parameterized Lee–Yang–Parr exchange functional (B3LYP) with 6-31G* basis sets.[23] The results show that the HOMO orbitals are distributed mostly on the diphenylsulfone core of **SPDP**, **SPDQ** and **SPPP** (Fig. 5a). This indicates that HOMO levels of the new sulfone-based ETMs are mainly determined by the $SO_2$ group. However, the LUMO orbitals of **SPDP** and **SPDQ** are dispersed throughout the whole molecule from $SO_2$ to the functional side groups whereas the LUMO orbital of **SPPP** is not distributed to the attached phenyl group. We can conclude that the LUMO orbital largely depends on the attached strong electron withdrawing group. Based on this, we expect that **SPDP** and **SPDQ** may have better electron transport properties than **SPPP**.

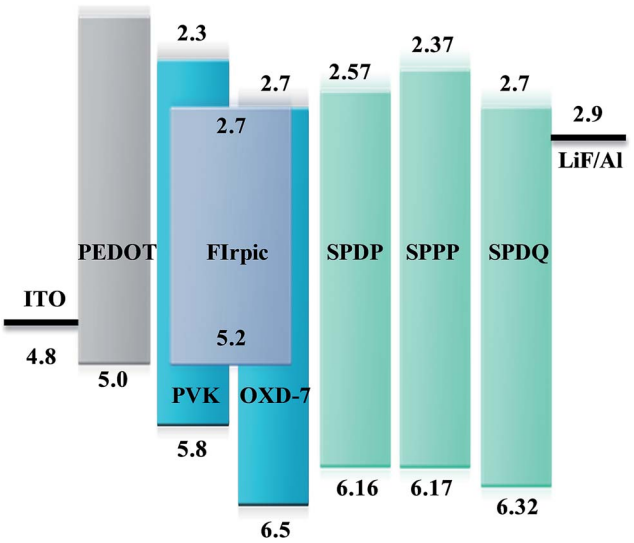


Fig. 4 Energy level diagram of the blue PhOLEDs with sulfone-based ETMs.

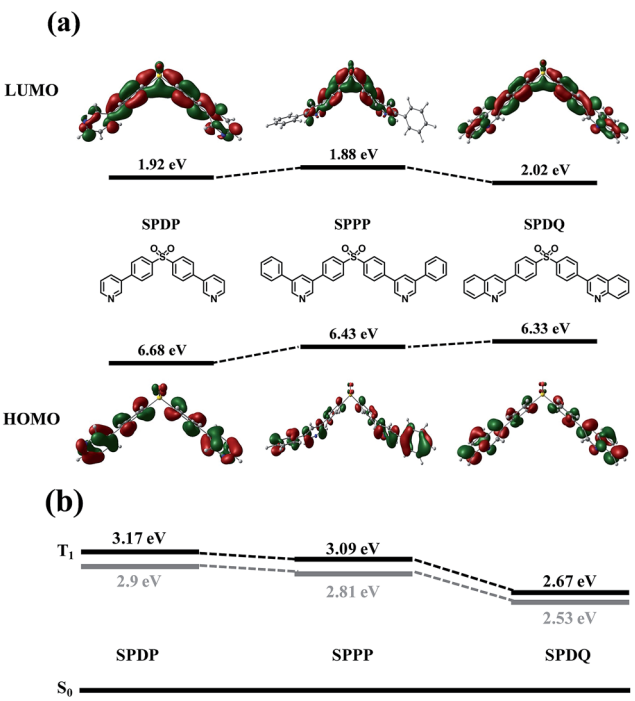


Fig. 5 (a) Calculated HOMO/LUMO energy levels and orbitals of SPDP, SPPP and SPDQ; (b) calculated (black bold lines) and measured (gray bold lines) triplet energy values of the sulfone-based ETMs.

The calculated triplet energy values of these molecules are shown in Fig. 5b in comparison with the measured triplet energy values of the sulfone-based ETMs. The results indicate that the calculated triplet energy values of **SPDP**, **SPPP** and **SPDQ**, which are 3.17, 3.09 and 2.67 eV, respectively, are very close to the measured values. The calculated and measured $E_T$ values agree to within 5–10%, which is very good. **SPDP** and **SPPP** with phenyl and phenylpyridine substituents combine a high triplet energy with a wide band gap because those substituents do not affect the overall conjugation length, while the triplet energy value of **SPDQ** decreased significantly due to the extended conjugation length through attached quinoline rings. These results suggest that DFT calculation of electronic structure including the triplet energy can be a promising strategy to designing new high triplet energy electron transport materials for highly efficient PhOLEDs.

### Space-charge-limited current (SCLC) carrier mobility

We investigated the electron transport properties of the sulfone-based materials by space-charge-limited current (SCLC) measurement of the electron mobility. The current density–voltage (*J*–*V*) characteristics of the SCLC devices with the structure of ITO/sulfone-based ETM (100 nm)/Al are shown in Fig. 6. The sulfone-based ETMs were thermally vacuum-evaporated to form 100 nm thick layers followed by Al deposition. The electron mobility was extracted by fitting the current density–voltage (*J*–*V*) curves in the near quadratic region according to the modified Mott–Gurney equation,[24]

$$J = \frac{9}{8}\varepsilon\varepsilon_0\mu\frac{V^2}{L^3}\exp\left(0.89\beta\frac{\sqrt{V}}{\sqrt{L}}\right)$$

where $J$ is the current density, $\varepsilon_0$ is the permittivity of free space, $\varepsilon$ is the relative permittivity, $\mu$ is the zero-field mobility, $V$ is the applied voltage, $L$ is the thickness of active layer, and $\beta$ is the field-activation factor. We fixed the maximum electric field at $3.0 \times 10^5$ V cm$^{-1}$. The zero-field electron mobility of **SPDP** was found to be $5.9 \times 10^{-6}$ cm$^2$ V$^{-1}$ s$^{-1}$ ($\beta = 3.9 \times 10^{-5}$ cm$^{1/2}$ V$^{-1/2}$) whereas the value for **SPDQ** was $1.6 \times 10^{-6}$ cm$^2$ V$^{-1}$ s$^{-1}$ ($\beta = 4.7 \times 10^{-5}$ cm$^{1/2}$ V$^{-1/2}$). The electron mobility of **SPDP** is higher than that of **SPDQ** although they are of the same order of magnitude. However, **SPPP** showed a relatively low electron

 

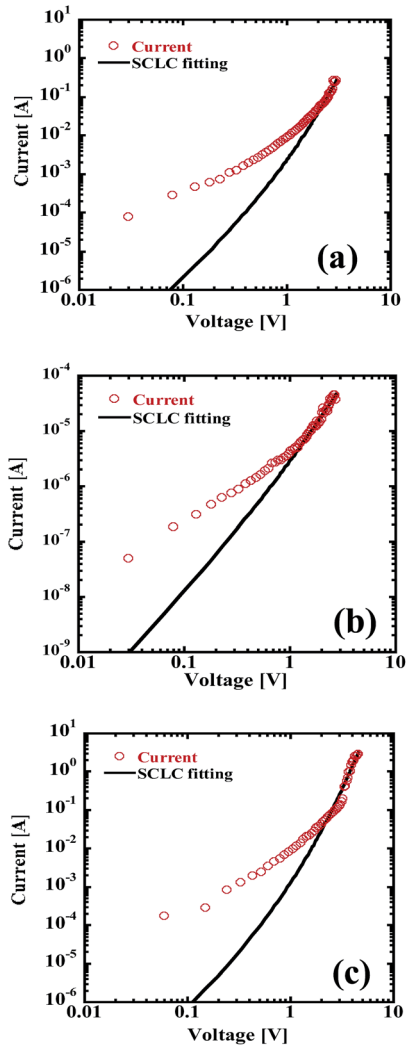


Fig. 6 Current–voltage characteristics of the SCLC devices with the structure of ITO/sulfone-based ETM (100 nm)/Al; (a) SPDP; (b) SPPP; and (c) SPDQ.

mobility of $7.3 \times 10^{-8}$ cm$^2$ V$^{-1}$ s$^{-1}$ ($\beta = 1.3 \times 10^{-5}$ cm$^{1/2}$ V$^{-1/2}$), which is two orders of magnitude lower than the electron mobility of **SPDP** and **SPDQ**. The low carrier mobility in **SPPP** could be due to the poor intermolecular interactions as a result of the phenyl groups on each side. Attached phenyl ring disturbs planar molecular structure and thus hinders efficient molecular packing.

### Blue PhOLEDs with sulfone-based electron transport layer

To evaluate electron-transport and exciton blocking ability of the new sulfone-based ETMs, we initially fabricated PhOLEDs with **SPDP** ETL. In order to optimize device performance, the thickness of **SPDP** ETL was varied as 5, 15, and 30 nm in blue PhOLEDs. Fig. 7 shows the electrical characteristics and performance of PhOLEDs with different thicknesses of **SPDP**. The PhOLEDs with 5 and 15 nm thick **SPDP** showed similar current densities whereas the device with 30 nm thick **SPDP** showed a lower current density due to its much larger thickness.

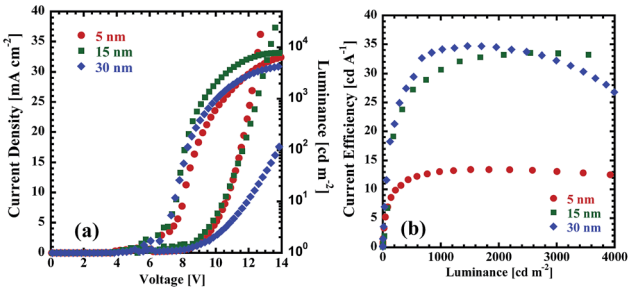


Fig. 7 (a) Current density–voltage–luminance ($J$–$V$–$L$) characteristics (b) current efficiency–luminance (CE–$L$) of blue PhOLEDs with different thicknesses of SPDP ETL.

The maximum luminance (brightness) decreased with increasing thickness of the **SPDP** ETL. However, the performance of the PhOLEDs significantly increased with 15 and 30 nm **SPDP** ETL compared to the 5 nm ETL. The PhOLEDs with 5 nm thick **SPDP** showed a high turn-on voltage of 6.6 V and a current efficiency (CE) of 13.4 cd A$^{-1}$ (power efficiency (PE) = 3.9 lm W$^{-1}$). The performance of the PhOLEDs dramatically changes with thicker **SPDP** ETL (15 and 30 nm). PhOLEDs with 15 nm **SPDP** ETL showed a reduced turn-on voltage (5.2 V) and also a significantly increased efficiency (Fig. 7b). This represents a 2.5-fold higher efficiency compared to the device with 5 nm ETL thickness. As the thickness of **SPDP** increases to 30 nm, device showed a slightly higher turn-on voltage (5.5 V) compared to the device with 15 nm ETL thickness. The CE and PE of the PhOLEDs with 30 nm thick **SPDP** ETL was comparable to the device with 15 nm thick **SPDP**. Nevertheless, the current efficiency of the 30 nm **SPDP** device showed the highest value of 33.9 cd A$^{-1}$. The device with 15 nm **SPDP** ETL had a high current efficiency of 33.6 cd A$^{-1}$, which is similar to the 30 nm **SPDP** ETL device performance.

We could observe severe roll-off in efficiency in the PhOLED with 30 nm thick **SPDP** whereas the device with 15 nm thick **SPDP** showed a reduced roll-off in efficiency at high luminance.

Electroluminescence (EL) spectra of all the blue PhOLEDs with different thicknesses of **SPDP** are shown in Fig. 8. The EL spectra showed that[10] the blue emission originated from FIrpic triplet emitter with the maximum peak at 472 nm. We can

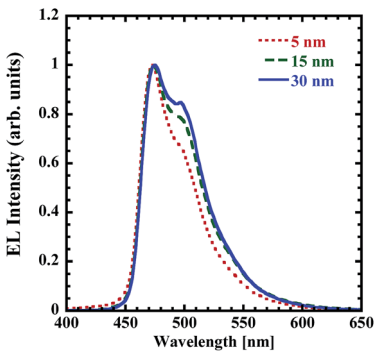


Fig. 8 Normalized EL spectra of the blue PhOLEDs with different thicknesses of SPDP ETL.

clearly see the EL intensity of shoulder peak around 500 nm increases as the thickness of **SPDP** increases. The increased EL intensity of the shoulder peak is due to a microcavity effect,[25] which is also consistent with the increased device performance. Commission Internationale de L'Eclairage (CIE) 1931 coordinates of the devices changed from (0.13, 0.28) to (0.14, 0.34) when the thickness of **SPDP** changed from 5 to 30 nm. This result imply that although increased EL intensity of the shoulder peak around 500 nm is effective for the enhancement of the device performance, there is an undesirable change in the purity of blue color due to the green emission. Therefore, we consider the 15 nm thickness as the optimum for high efficiency and low roll-off in efficiency for blue PhOLEDs using sulfone-based ETMs.

We fabricated blue PhOLEDs with all the sulfone-based ETMs (**SPDP**, **SPPP**, and **SPDQ**) with the ETL thickness fixed at 15 nm. Standard device configuration for the blue PhOLEDs were ITO/PEDOT:PSS/PVK:OXD-7:FIrpic/ETM/LiF/Al. Four different series of PhOLEDs were fabricated to investigate the effect of high triplet energy, electron mobility and energy levels on device performance. Device I had no ETL and devices II, III, and IV had **SPDP**, **SPPP**, and **SPDQ** ETL, respectively.

The current density–voltage–luminance (*J*–*V*–*L*), and current efficiency–luminance (CE–*L*) characteristics of PhOLEDs with sulfone-based ETMs as the electron transport layer are shown in Fig. 9. PhOLEDs with sulfone-based ETLs all showed enhanced device performance (devices II, III, and IV) compared to the device without ETL (device I) as shown in Fig. 9 and Table 2. Device II showed a significantly reduced turn-on voltage (5.2 V) and had an increased current efficiency (CE) of 33.6 cd $A^{-1}$ with an external quantum efficiency (EQE) of 19.6%, while device I showed a high turn-on voltage (6.3 V) and a CE of 16.2 cd $A^{-1}$ with an EQE of 10.2%. The device with **SPDP** ETL showed much higher performance than using commercial BPhen ETL (CE = 16.5 cd $A^{-1}$, EQE = 8.4%).[4b] Devices III and IV also had enhanced device performance, showing CE of 27.1 and 30.6 cd $A^{-1}$ (EQE = 13.9 and 15.7%), respectively. However, the maximum luminance of device IV was much lower than that of device II and device III, which is presumably due to the low current density. Comparing the current densities, device II showed the highest current density and the device IV showed the lowest current density, which can be correlated with the energy levels of the sulfone-based ETMs. **SPDP** has an energy barrier of only 0.27 eV with PVK-based polymeric host material (Fig. 4), whereas **SPDQ** has a large energy barrier of 0.4 eV with the host material. Although the energy barrier between **SPPP** and PVK host material is very small (0.07 eV), the electron mobility of **SPPP** is very low ($\sim 10^{-8}$ $cm^2$ $V^{-1}$ $s^{-1}$) compared to the **SPDP** and **SPDQ** ($\sim 10^{-6}$ $cm^2$ $V^{-1}$ $s^{-1}$), which is consistent with the performance of the blue PhOLEDs.

Device IV with **SPDQ** also showed significantly enhanced device performance despite the relatively low triplet energy value of **SPDQ** ($E_T$ = 2.53 eV) compared to the other high triplet energy sulfone-based ETMs (**SPDP**, $E_T$ = 2.90 eV and **SPPP**, $E_T$ = 2.81 eV). We note that in order to confine triplet excitons effectively inside the EML, the triplet energy of ETL should be higher than that of the FIrpic emitter (2.7 eV).[8,26] Nevertheless, **SPDQ** ETL with a low triplet energy significantly improved the PhOLED efficiency, which implies that facilitating electron transport to achieve better charge carrier balance in the emission layer by an ETM with high electron mobility is also an important factor that can lead to high performance PhOLEDs even without a high triplet energy. Furthermore, EL spectrum of device IV with **SPDQ** ETL showed blue emission with very weak shoulder peak around 500 nm with CIE coordinates of (0.13, 0.28) while the EL spectrum of device III with **SPPP** ETL had a more prominent shoulder peak with CIE coordinates (0.14, 0.32) with unwanted greenish emission (Fig. 10). These results suggest that an appropriate LUMO level of the ETM is essential while high electron mobility is also important to facilitate electron-transport to achieve high-performance PhOLEDs.

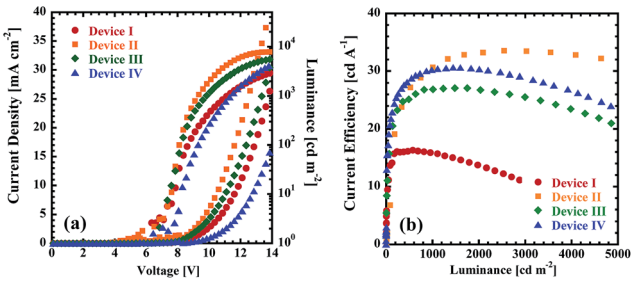


Fig. 9 (a) Current density–voltage–luminance (*J*–*V*–*L*) of blue PhOLEDs with sulfone-based ETLs. (b) Current efficiency–luminance (CE–*L*) of blue PhOLEDs with sulfone-based ETMs.

Table 2 Device characteristics of blue PhOLEDs based on sulfone-based ETMs[a]

| Device | ETL | $V_{on}$[b] [V] | Drive voltage [V] | Current density [mA $cm^{-2}$] | Luminance [cd $m^{-2}$] | Current efficiency [cd $A^{-1}$] | Power efficiency [lm $W^{-1}$] | External quantum efficiency [%] |
|---|---|---|---|---|---|---|---|---|
| Device I | None | 6.3 | 15.4 | 53.4 | 3490 | 6.5 | 1.3 | 4.1 |
| | | | *9.8* | *2.2* | *360* | *16.2* | *4.1* | *10.2* |
| Device II | **SPDP** | 5.2 | 13.8 | 39.6 | 7810 | 19.2 | 4.3 | 11.2 |
| | | | *10.4* | *33.4* | *2730* | *33.6* | *10.6* | *19.6* |
| Device III | **SPPP** | 6.7 | 15.4 | 49.7 | 6010 | 12.1 | 2.1 | 6.2 |
| | | | *10.0* | *4.1* | *1100* | *27.1* | *8.9* | *13.9* |
| Device IV | **SPDQ** | 6.3 | 14.8 | 37.2 | 5990 | 16.1 | 3.2 | 7.3 |
| | | | *10.2* | *4.5* | *1390* | *30.6* | *8.2* | *15.7* |

[a] Values in *italic* correspond to those at maximum device efficiencies. [b] Turn-on voltage (at luminance of ~1 cd $m^{-2}$).

 

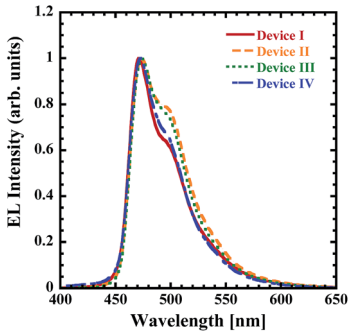


Fig. 10 Normalized EL spectra of the blue PhOLEDs with sulfone-based ETMs.

## Conclusion

A series of new sulfone-based electron transport materials with high triplet energies and wide band gaps are synthesized, characterized and demonstrated to lead to highly efficient blue PhOLEDs. The combination of a diphenylsulfone core with electron withdrawing end groups such as pyridine, phenylpyridine, and quinoline is found to be effective in achieving a high triplet energy (2.8–2.9 eV) and a wide energy gap (3.6–3.8 eV), resulting in efficient exciton/hole blocking with good electron-transport characteristics. SCLC derived electron mobility was (2–6) $\times 10^{-6}$ $cm^2 V^{-1} s^{-1}$ for **SPDP** and **SPDQ** thin films but was significantly lower in the case of **SPPP** ($7 \times 10^{-8}$ $cm^2 V^{-1} s^{-1}$). Density functional theory (DFT) calculated triplet energy values of the sulfone-based materials were found to be in good agreement (within 5–10%) of experimental values measured from low temperature phosphorescence spectra. Blue PhOLEDs incorporating the new sulfone-based materials as an electron transport layer had a significantly enhanced performance with a current efficiency of up to 33.6 cd $A^{-1}$ and external quantum efficiency of 19.6%. The results suggest that sulfone-based electron transport materials are promising for achieving high-performance phosphorescent optoelectronic devices.

## Acknowledgements

This work was supported by Solvay S. A. and in part by the Boeing-Martin Professorship.

## Notes and references

1 S. Reineke, F. Lindner, G. Schwartz, N. Seidler, K. Walzer, B. Lüssem and K. Leo, *Nature*, 2009, **459**, 234.
2 M. A. Baldo, D. F. Obrien, Y. You, A. Shoustikov, S. Sibley, M. E. Thompson and S. R. Forrest, *Nature*, 1998, **395**, 151.
3 L. Xiao, S.-J. Su, Y. Agata, H. Lan and J. Kido, *Adv. Mater.*, 2009, **21**, 1271.
4 (*a*) T. Earmme and S. A. Jenekhe, *J. Mater. Chem.*, 2012, **22**, 4660; (*b*) T. Earmme and S. A. Jenekhe, *Adv. Funct. Mater.*, 2012, **22**, 5126; (*c*) T. Earmme and S. A. Jenekhe, *Appl. Phys. Lett.*, 2013, **102**, 233305.
5 N. Chopra, J. Lee, Y. Zheng, S.-H. Eom, J. Xue and F. So, *Appl. Phys. Lett.*, 2008, **93**, 143307.
6 S. O. Jeon and J. Y. Lee, *J. Mater. Chem.*, 2012, **22**, 4233.
7 A. P. Kulkarni, C. J. Tonzola, A. Babel and S. A. Jenekhe, *Chem. Mater.*, 2004, **16**, 4556.
8 (*a*) H. Sasabe, E. Gonmori, T. Chiba, Y.-J. Li, D. Tanaka, S.-J. Su, T. Takeda, Y.-J. Pu, K.-I. Nakayama and J. Kido, *Chem. Mater.*, 2008, **20**, 5951; (*b*) H. Sasabe, T. Chiba, S.-J. Su, Y.-J. Pu, K.-I. Nakayama and J. Kido, *Chem. Commun.*, 2008, 5821.
9 (*a*) S.-J. Su, H. Sasabe, Y.-J. Pu, K.-I. Nakayama and J. Kido, *Adv. Mater.*, 2010, **22**, 3311; (*b*) H. Inomata, K. Goushi, T. Masuko, T. Konno, T. Imai, H. Sasabe, J. J. Brown and C. Adachi, *Chem. Mater.*, 2004, **16**, 1285.
10 (*a*) T. Earmme, E. Ahmed and S. A. Jenekhe, *Adv. Mater.*, 2010, **22**, 4744; (*b*) E. Ahmed, T. Earmme and S. A. Jenekhe, *Adv. Funct. Mater.*, 2011, **21**, 3889.
11 P. E. Burrows, A. B. Padmaperuma, L. S. Sapochak, P. Djurovich and M. E. Thompson, *Appl. Phys. Lett.*, 2006, **88**, 183503.
12 (*a*) S. O. Jeon, K. S. Yook, C. W. Joo and J. Y. Lee, *J. Phys. D: Appl. Phys.*, 2009, **42**, 225103; (*b*) S. O. Jeon, K. S. Yook, C. W. Joo and J. Y. Lee, *J. Mater. Chem.*, 2009, **19**, 5940.
13 B. Lu, Y. Li and J. Xu, *J. Electroanal. Chem.*, 2010, **643**, 67.
14 (*a*) C. J. Tonzola, M. M. Alam and S. A. Jenekhe, *Adv. Mater.*, 2002, **14**, 1086; (*b*) C. J. Tonzola, A. P. Kulkarni, A. P. Gifford, W. Kaminsky and S. A. Jenekhe, *Adv. Funct. Mater.*, 2007, **17**, 863; (*c*) A. P. Kulkarni, A. P. Gifford, C. J. Tonzola and S. A. Jenekhe, *Appl. Phys. Lett.*, 2005, **86**, 061106.
15 F.-M. Hsu, C.-H. Chien, Y.-J. Hsieh, C.-H. Wu, C.-F. Shu, S.-W. Liub and C.-T. Chen, *J. Mater. Chem.*, 2009, **19**, 8002.
16 S.-J. Kim, J. Leroy, C. Zuniga, Y. Zhang, L. Zhu, J. S. Sears, S. Barlow, J.-L. Brédas, S. R. Marder and B. Kippelen, *Org. Electron.*, 2011, **12**, 1314.
17 H. Sasabe, Y. Seino, M. Kimura and J. Kido, *Chem. Mater.*, 2012, **24**, 1404.
18 (*a*) Q. Zhang, B. Li, S. Huang, H. Nomura, H. Tanaka and C. Adachi, *Nat. Photonics*, 2014, **8**, 326; (*b*) Q. Zhang, J. Li, K. Shizu, S. Huang, S. Hirata, H. Miyazaki and C. Adachi, *J. Am. Chem. Soc.*, 2012, **134**, 14706.
19 A. P. Kulkarni and S. A. Jenekhe, *Macromolecules*, 2003, **36**, 5285.
20 M. A. Baldo and S. R. Forrest, *Phys. Rev. B: Condens. Matter Mater. Phys.*, 2000, **62**, 10958.
21 A. K. Agrawal and S. A. Jenekhe, *Chem. Mater.*, 1996, **8**, 579.
22 D. Young, *Computational Chemistry: A Practical Guide for Applying Techniques to Real World Problems*, John Wiley & Sons, Inc, New York, USA, 2001.
23 W. J. Hehre, R. Ditchfie and J. A. Pople, *J. Chem. Phys.*, 1972, **56**, 2257.
24 (*a*) P. N. Murgatroyd, *J. Phys. D: Appl. Phys.*, 1970, **3**, 1488; (*b*) N. F. Mott and D. Gurney, *Electronic Processes in Ionic Crystals*, Academic Press, New York, USA, 1970.
25 F. So, B. Krummacher, M. K. Mathai, D. Poplavskyy, S. A. Choulis and V.-E. Choong, *J. Appl. Phys.*, 2007, **102**, 091101.
26 S.-J. Su, Y. Takahashi, T. Chiba, T. Takeda and J. Kido, *Adv. Funct. Mater.*, 2009, **19**, 1260.